Available online at www.derpharmachemica.com

ISSN 0975-413X
CODEN (USA): PCHHAX

Der Pharma Chemica, 2016, 8(2):172-190
(http://derpharmachemica.com/archive.html)

Pyridinium derivatives as corrosion inhibitors for mild steel in 1M HCl: Electrochemical, surface and quantum chemical studies

H. Lgaz[1], O. Benali[2], R. Salghi[3,*], S. Jodeh[4], M. Larouj[1], O. Hamed[4], M. Messali[5], S. Samhan[6], M. Zougagh[7,8] and H. Oudda[1]

[1]*Laboratory Separation Processes, Faculty of Science, University Ibn Tofail, Kenitra, Morocco*
[2]*Department of biology, Faculty of sciences, University Dr. Tahar Moulay – Saïda- Algeria*
[3]*Laboratory of Applied Chemistry and Environment, ENSA, Université Ibn Zohr, Agadir, Morocco*
[4]*Department of Chemistry, An-Najah National University, Nablus, Palestine*
[5]*Chemistry Department, Faculty of Science, Taibah University, Al-Madinah Al-Mounawwara, Saudi Arabia*
[6]*Palestine Water Authority, Ramallah, Palestine*
[7]*Regional Institute for Applied Chemistry Research, IRICA, E-13004, Ciudad Real, Spain*
[8] *Castilla-La Mancha Science and Technology Park, E-02006, Albacete, Spain*

ABSTRACT

Pyridinium derivatives namely, 4-(dimethylamino)-1-ethylpyridinium bromide (DEB), 4-(dimethylamino)-1-pentylpyridinium bromide (DPB) synthesised by our group, were tested as inhibitors for the corrosion of mild steel in 1 M HCl using polarisation and electrochemical impedance measurements, Scanning electron microscope (SEM) and Quantum chemical calculations. The results show that the DEB and DPB enhances inhibition at all concentrations. The best protection (94.09%) is obtained by adding DEB at 10^{-4} M. Polarisation curves show that DEB and DPB acts as a mixed type inhibitor. The degree of the surface coverage of the adsorbed inhibitors is determined by weight loss measurement, and it was found that the adsorption of the two compounds on the mild steel surface obeys the Langmuir adsorption isotherm. The effect of the temperature on the corrosion behaviour with addition of DEB and DPB at various concentrations was studied in the temperature range 303 – 333 K. Results show that the rate of corrosion of mild steel increased and protection efficiency decreased with increasing temperature. Kinetic parameters as well as thermodynamic parameters were calculated and discussed. Scanning electron microscopy (SEM) was applied to study the mild steel surface in the presence and absence of the two compounds. Quantum chemical calculations using DFT at the B3LYP/6-31G level of theory was further used to calculate some electronic properties of the molecule in order to ascertain any correlation between the inhibitive effect and molecular structure of the DEB and DPB.*

Keywords: Pyridinium derivatives; Mild steel; Inhibition corrosion; Hydrochloride acid.

INTRODUCTION

The use of inhibitors is one of the most important tasks for protection of metals against corrosion in acidic media [1-3], for this reason, many works on inhibitors have been carried out, especially on hetero atoms containing inhibitors and rapid progress has been made in this field in recent years [4-6]. The synthesis of new organic molecules offers different molecular structures containing several heteroatoms and substituents and their adsorption is generally explained by the formation of an adsorptive film of a physical or chemical character on the metal surface [7-9]. In recent times, in our group, attention has been paid to the development of new organic compounds as acid inhibitors [10-12]. In continuation of our work, we have synthesised organic compounds namely 4-(dimethylamino)-1-ethylpyridinium bromide (DEB), 4-(dimethylamino)-1-pentylpyridinium bromide (DPB) with a view to study their

ability to inhibit mild steel in hydrochloric acid. It should be noted that, the choice of these compounds is based on molecular structure considerations. The introduction of ethyl and pentyl group changes essentially the volume of the 4-dimethylaminopyridinium bromide molecule and hence the surface occupied when adsorbing at the metal. The effects of compounds concentrations on the values of the corrosion parameters characterising the systems have been recorded by weight loss measurements and electrochemical methods (potentiodynamic polarisation curves and electrochemical impedance spectroscopy). Scanning electron microscope (SEM) and Quantum chemical calculations were also utilized to investigate the corrosion protection performance of DEB and DPB on mild steel in the aggressive solution. The free energy, the enthalpy and entropy for the adsorption process and the apparent activation energies for the dissolution process were also determined in the absence and the presence of the two inhibitors.
The molecular structure of 4-(dimethylamino)-1-ethylpyridinium bromide (DEB), 4-(dimethylamino)-1-pentylpyridinium bromide (DPB is as shown below (Fig. 1) :

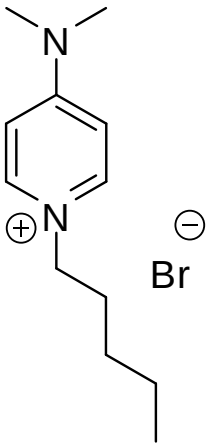

4-(dimethylamino)-1-pentylpyridinium bromide (**DPB**)

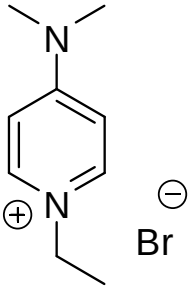

4-(dimethylamino)-1-ethylpyridinium bromide (**DEB**)

Figure .1. The molecular structure of DBP and DEB

MATERIALS AND METHODS

2.1. Procedure for the preparation of pyridinium ionic liquids DPB and DEB using conventional method

4-(dimethylamino) pyridine (1eq) and 1-bromopentane or bromoethane (1.1eq) were added to toluene and stirred at 80 °C for 18 h. The reaction was deemed complete when oil or a solid separated from the initial clear and homogenous mixture. Unreacted starting materials and solvent were removed by extraction or filtration. The pyridinium salt was then washed with ethyl acetate and dried *in vacuo* to remove all VOCs.

4-(dimethylamino) pyridine (1 eq) and the appropriate alkyl halide (1 eq) were placed in a closed vessel and exposed to irradiation for 5 h at 70 °C in a sonicator. The product was then isolated and purified as described in the previous procedure.

White crystals (DPB), Mp 210-215 ºC, ^{1}H NMR (D_2O, 400 MHz,): δ = 0.74 (t, 3H), 1.18 (m, 4H), 1.73 (sixtet, 2H), 3.09 (s, 6H), 4.02 (t, 2H), 6.77 (d, 2H), 7.91 (d, 2H); ^{13}C NMR (D_2O, 100 MHz,): δ = 13.1 (CH_3), 21.4 (CH_2), 27.4 (CH_2), 29.7 (CH_2), 39.4 (CH_3) 57.6 (CH_2), 107.5 (CH), 141.3 (CH), 156.2 (C); LCMS (M-Br) 193.3 found for $C_{12}H_{21}N_2^+$.

White crystals (DEB), Mp 130-132 ºC, ^{1}H NMR ($CDCl_3$, 400 MHz,): δ = 1.36 (t, 3H), 3.08 (s, 6H), 4.06 (t, 2H), 6.78 (d, 2H), 7.94 (d, 2H); ^{13}C NMR ($CDCl_3$, 100 MHz,): δ = 15.2 (CH_3), 39.6 (CH_3), 52.9 (CH_2), 107.6 (CH), 140.9 (CH), 156.2 (C); LCMS (M-Br) 151.2 found for $C_9H_{15}N_2^+$.

2.2. Solutions

The aggressive solutions of 1.0 M HCl were prepared by dilution of analytical grade 37% HCl with distilled water. The solution tests are freshly prepared before each experiment. The organic compounds tested were 4-(dimethylamino)-1-ethylpyridinium bromide (DEB) and 4-(dimethylamino)-1-pentylpyridinium bromide (DPB). The concentration range of this compound was 10^{-4} to 5.10^{-6} M.

2.3. Weight loss measurements

Coupons were cut into 2 × 2 × 0.08 cm^3 dimensions are used for weight loss measurements. Prior to all measurements, the exposed area was mechanically abraded with 180, 320, 800, 1200 grades of emery papers. The specimens were washed thoroughly with bidistilled water, degreased and dried with ethanol. Gravimetric measurements are carried out in a double walled glass cell equipped with a thermostated cooling condenser. The solution volume is 80 mL. The immersion time for the weight loss is 6 h at 298 K.

2.4. Electrochemical measurements

2.4.1. Electrochemical impedance spectroscopy (EIS)

The electrochemical measurements were carried out using Voltalab (Tacussel-Radiometer PGZ 100) potentiostat and controlled by Tacussel corrosion analysis software model (Voltamaster 4) under static condition. The corrosion cell used had three electrodes. The reference electrode was a saturated calomel electrode (SCE). A platinum electrode was used as auxiliary electrode. The working electrode was carbon steel. All potentials given in this study were referred to this reference electrode. The working electrode was immersed in test solution for 30 minutes to establish asteady state open circuit potential (E_{ocp}). After measuring the Eocp, the electrochemical measurements were performed. All electrochemical tests have been performed in aerated solutions at 298 K. The EIS experiments were conducted in the frequency range with high limit of 100 kHz and different low limit 0.1 Hz at open circuit potential, with 10 points per decade, at the rest potential, after 30 min of acid immersion, by applying 10 mV ac voltage peak-to-peak. Nyquist plots were made from these experiments. The best semicircle can be fit through the data points in the Nyquist plot using a non-linear least square fit so as to give the intersections with the **x**-axis.

2.4.2. Potentiodynamic polarization

The electrochemical behaviour of carbon steel sample in inhibited and uninhibited solution was studied by recording anodic and cathodic potentiodynamic polarization curves. Measurements were performed in the 1.0 M HCl solution containing different concentrations of the tested inhibitor by changing the electrode potential automatically from -800 mV to -200 mV versus corrosion potential at a scan rate of 1 $mV.s^{-1}$. The linear Tafel segments of anodic and cathodic curves were extrapolated to corrosion potential to obtain corrosion current densities (I_{corr}).

2.5. Quantum chemical calculations

Quantum chemical calculations are very effective methods for determining a correlation between molecular structure and inhibition efficiency. They can also be utilized to support the accuracy of experimental results [13-15]. Thus, it is important to compute the quantum chemical parameters, such as the energy of the highest occupied molecular orbital (E_{HOMO}), the energy of the lowest unoccupied molecular orbital (E_{LUMO}), the fraction of electrons transferred (ΔN) and the energies of the frontier molecular orbitals. In the present study, density functional theory (DFT) was used to determine the molecular structure of DPB and DEB as a corrosion inhibitor for mild steel. The corrosion inhibition behavior of DPB and DEB on the inhibitors in acidic solution was investigated using some experimental techniques. Quantum chemical computations were carried out by density function theory (DFT) with 6-31-G (d, p) basis set. All of the calculations were carried out with Gaussian 03W package [16-17]. The following quantum chemical parameters were acquired: E_{HOMO}, E_{LUMO}, E_{HOMO} - E_{LUMO} energy gap (ΔE), electronegativity (χ), global hardness (η), global softness (σ), fraction of electrons transferred (ΔN) and Mulliken charges on the backbone atoms.

2.6. Scanning electron microscopy (SEM)

Immersion corrosion analysis of steel samples in the acidic solutions with and without the optimal concentration of the inhibitor was performed using SEM. Immediately after the corrosion tests, the samples were subjected to SEM studies to know the surface morphology using SEM Jeol JSM-5800 scanning electron microscope.

RESULTS AND DISCUSSION

3.1. Weight loss measurements

3.1.1. Effect of temperatures

Temperature has a great effect on the corrosion phenomenon and generally the corrosion rate increases with the rise of the temperature. For this reason, we have studied the temperature influence on the efficiency of the two compounds. We made weight-loss measurements in the range of temperature 303–333 K, in the absence and presence of DPB and DEB at different concentrations of these inhibitors after 6 hours of immersion. The corresponding data are shown in Table 1. The corrosion rate (W) was calculated from the following equation:

$$W = \frac{m_1 - m_2}{S.t} \quad (1)$$

where m_1 is the mass of the specimen before corrosion, m_2 the mass of the specimen after corrosion, S the total area of the specimen, t the corrosion time and W the corrosion rate.

Table 1 Corrosion rate and inhibition efficiency obtained from weight loss measurements of inhibitors in 1 M HCl containing various concentrations of DPB and DEB at different temperatures.

	Conc. (M)	Temperature (°C)							
		30		40		50		60	
		W (*)	IE_w (%)	W (*)	IE_w (%)	W (*)	IE_w (%)	W (*)	IE_w (%)
Blank	1.0	1.135	---	2.466	---	5.032	---	10.029	----
DPB	10^{-4}	0.067	**94.09**	0.196	**92.05**	0.598	**88.12**	1.692	**83.13**
	5.10^{-5}	0.090	92.07	0.264	89.29	0.751	85.07	2.097	79.09
	10^{-5}	0.124	89.07	0.340	86.21	0.903	82.05	2.403	76.04
	5.10^{-6}	0.168	85.19	0.439	82.19	1.452	71.14	3.579	64.31
DEB	10^{-4}	0.122	**89.25**	0.362	**85.32**	0.866	**82.79**	2.098	**79.08**
	5.10^{-5}	0.145	87.22	0.405	83.58	1.003	80.07	2.410	75.97
	10^{-5}	0.191	83.17	0.539	78.14	1.146	77.22	2.638	73.70
	5.10^{-6}	0.259	77.18	0.661	73.19	1.493	70.33	3.412	65.98

(*): mg cm^{-2} h^{-1}

With the calculated corrosion rate, the inhibition efficiency of inhibitor for the corrosion of mild steel was obtained by using the following equation:

$$IE_W = \frac{W_1 - W_2}{W_1} x100 \quad (2)$$

where W_1 and W_2 are the corrosion rate of steel samples with and without the inhibitor, respectively.
The degree of surface coverage (Θ) was calculated using equation 3:

$$\Theta = 1 - \frac{W_2}{W_1} \quad (3)$$

The results show that the inhibition efficiency decreases with increasing temperature indicating that higher temperature dissolution of steel predominates on adsorption of the inhibitors at the surface. Is clear that, the inhibition efficiency increased with increase in inhibitors concentrations. The maximum value of inhibition efficiency obtained for 10^{-4} M is 94.09% and 89.25% for DPB and DEB at 308 K, respectively.

The Arrhenius plot and transition state plot were used to determine the activation energy (E_a), activation enthalpy ($\Delta H_a°$), and activation entropy ($\Delta S_a°$) for the corrosion of mild steel in 1M HCl with and without the inhibitors. The activation energy can be obtained by the Arrhenius equation and Arrhenius plot:

$$W = A \exp\left(\frac{-E_a}{RT}\right) \quad (4)$$

where W is the corrosion rate, R the gas constant, T the absolute temperature, A the pre-exponential factor.
Using the logarithm:

$$Ln\, W = -\frac{E_a}{RT} + Ln\, A \quad (5)$$

The graph of *LnW* against 1/T gives a straight line with a slope of (-E**a**/R).

Figs. 2a and 2b show the Arrhenius plot for mild steel in 1M HCl in the presence and absence of the two compounds. E_a was calculated and tabulated in Table 3.

The transition state equation was used to calculate the ΔH_a^0 and ΔS_a^0 :

$$W = \frac{RT}{Nh} \exp\left(\frac{\Delta S_a^0}{R}\right) exp\left(-\frac{\Delta H_a^0}{RT}\right) \quad (6)$$

where N is Avogadro's number and h is Plank's constant.

Eq. (6) looks like an exponential multiplied by a factor that is linear in temperature.

However, the activation energy is itself a temperature dependent quantity as follows:

$$E_a = \Delta H_a^0 - T\, \Delta S_a^0 \quad (7)$$

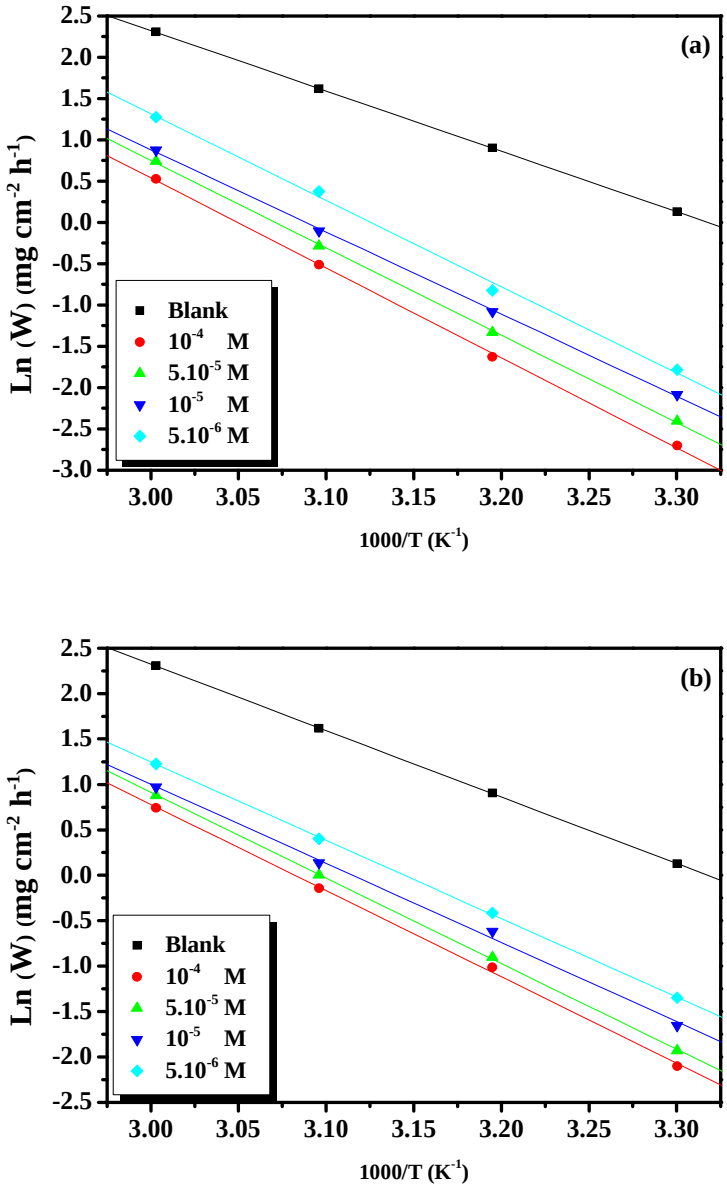

Fig. 2. Arrhenius plots for mild steel in 1 M HCl in the absence and presence of different concentrations of (a) DPB and (b) DEB

Table 2 Activation parameters for mild steel corrosion in 1M HCl in the absence and presence of different concentrations of DPB and DEB

Inhibitors	Conc. (M)	E_a (kJ mol^{-1})	ΔH_a^0 (kJ mol^{-1})	ΔS_a^0 (kJ mol^{-1}K^{-1})	E_a-ΔH_a^0
Blank	----	60.79	58.15	-51.84	2.64
DPB	10^{-4}	90.53	87.90	22.54	2.63
	5.10^{-5}	87.93	85.30	16.50	2.63
	10^{-5}	82.71	80.08	1.92	2.63
	5.10^{-6}	86.94	84.31	18.23	2.63
DEB	10^{-4}	78.93	76.29	-10.26	2.64
	5.10^{-5}	78.34	75.70	-10.95	2.64
	10^{-5}	72.43	69.79	-27.91	2.64
	5.10^{-6}	71.70	69.06	-28.07	2.64

Therefore, when all of the details are worked out one ends up with an expression that again takes the form of an Arrhenius exponential multiplied by a slowly varying function of T. The precise form of the temperature dependence depends upon the reaction, and can be calculated using formulas from statistical mechanics involving the partition functions of the reactants and of the activated complex [18].

Nevertheless, in order to carry simple calculations, Eq. (6) was rearranged to become:

$$Ln\left(\frac{W}{T}\right) = \left(\frac{-\Delta H_a^0}{RT}\right) + \left[Ln\left(\frac{R}{Nh}\right) + \frac{\Delta S_a^0}{R}\right] \quad (8)$$

A plot of Ln (W/T) against 1/T should give a straight line with a slope of (-ΔH_a^0/R) and intercept of $\left(\frac{R}{Nh}\right) + \frac{\Delta S_a^0}{R}$, as shown in Figs. 3a and 3b.

ΔH_a^0 and ΔS_a^0 were calculated and tabulated in Table 2. From this table, the activation energy E_a increases in the presence of the inhibitors. Increases in E_a with the presence of the two compounds indicate that a physical (electrostatic) adsorption occurred in the first stage. It should be noted that, DPB and DEB are an organic nitrogen compounds that give a cationic form in acid medium. The values of ΔH_a^0 and E_a are higher in the presence of the inhibitors. This indicates that the energy barrier of the corrosion reaction increased in the presence of the inhibitors without changing the mechanism of dissolution. The positive values of ΔH_a^0 for both corrosion processes with and without the inhibitors reveal the endothermic nature of the steel dissolution process and indicate that the dissolution of steel is difficult [19-20].

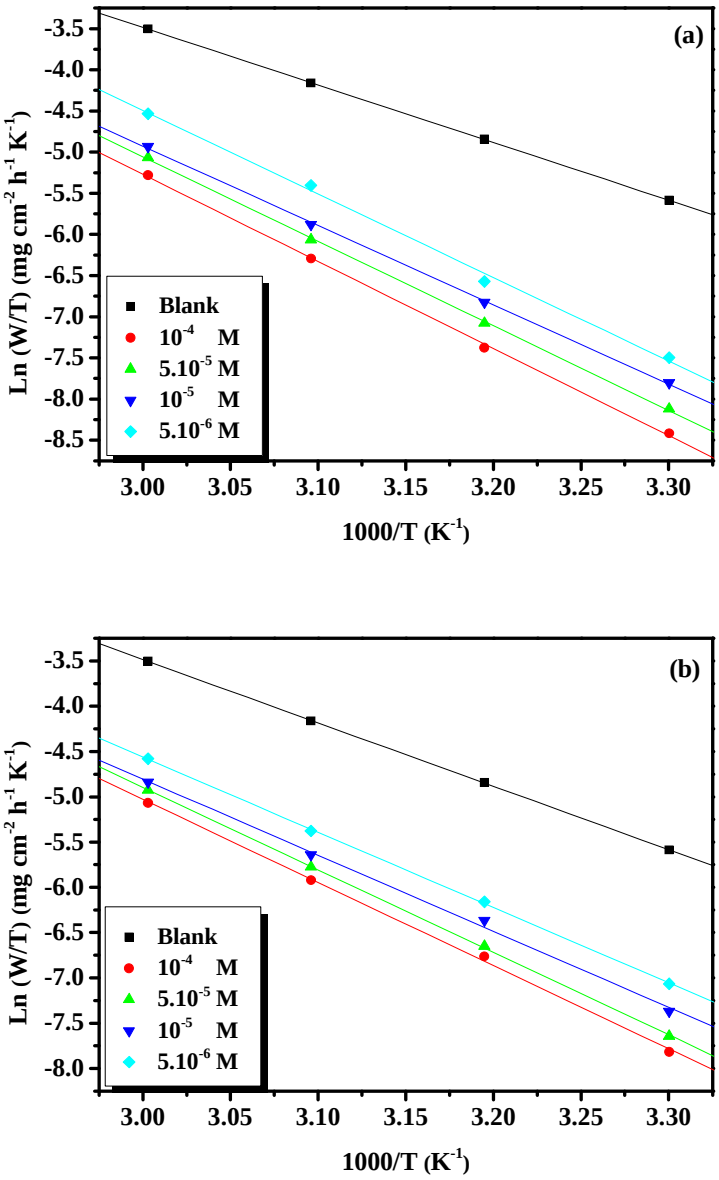

Fig. 3. Transition state plots for the inhibition of corrosion of inhibitors in 1M HCl in the absence and presence of different concentrations of (a) DPB and (b) DEB

The negative values of ΔS_a^0 imply that the disorderness is increased on going from reactant to product. It is observed that the shift of ΔS_a^0 to more positive values for DPB on increasing the concentration of the inhibitor is the driving force that can overcome the barriers for the adsorption of inhibitor onto the mild steel surface [21-22]. Also, for the second compound (DEB) the entropies of activation were positive indicating that the activation complex represents association steps and that the reaction was spontaneous and feasible [23-27].

3.1.3 Adsorption Isotherm and thermodynamic parameters

The degree of surface coverage values (θ) obtained from weight loss measurements using the equation (θ = E(%) / 100) assuming a direct relationship between surface coverage and inhibition efficiency were tested graphically by fitting to different isotherms. Attempts were made to fit θ values to the Freundlich, Temkin, Langmuir, and Flory-Huggins isotherms, and the correlation coefficient (R^2) values were used to determine the best fit isotherm. The best results were obtained for the Langmuir adsorption isotherm. The characteristics of the Langmuir adsorption isotherm are given by the equation:

$$\frac{C_{inh}}{\theta} = \frac{1}{K_{ads}} + C_{inh}$$

where C_{inh} is inhibitor concentration, K_{ads} is adsorption equilibrium constant for corrosion process. Figures 4a and 4b show the plots of Cinh/θ versus Cinh. The linear plots were obtained indicating that the experimental data obtained from three different measurements fits the Langmuir adsorption isotherm.

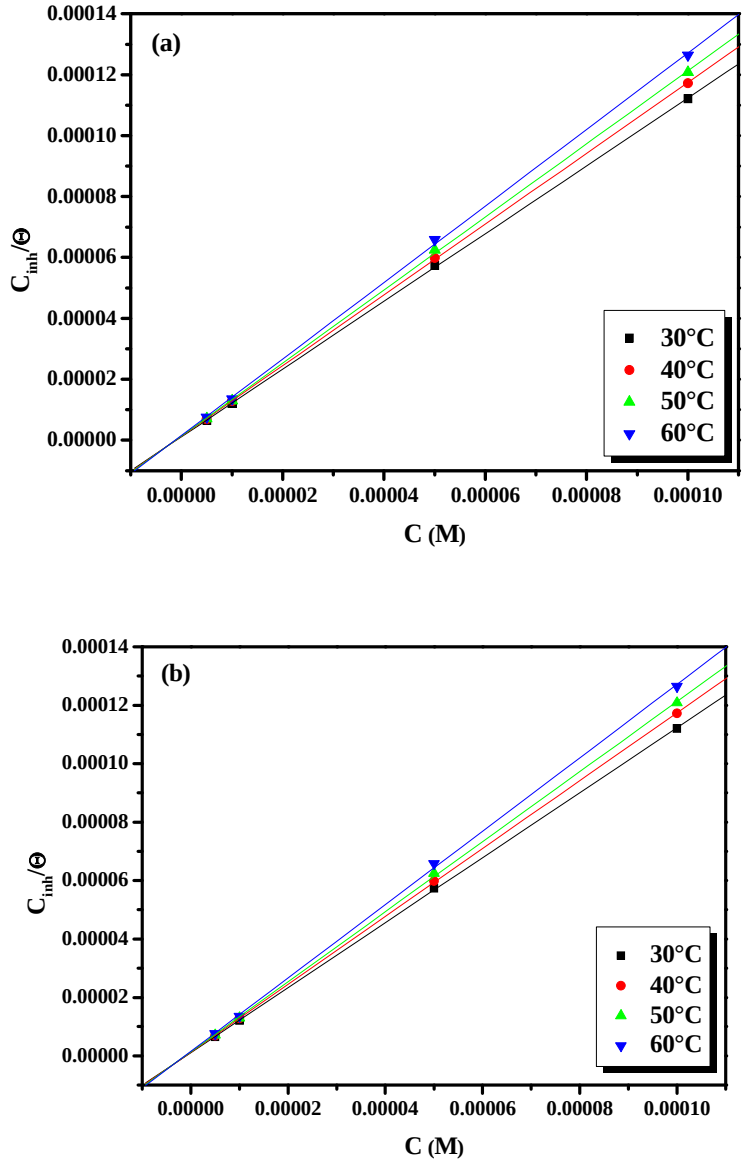

Fig. 4. Langmuir adsorption isotherm on mild steel in 1 M HCl at different temperatures of (a) DPB (b) DEB

The K_{ads} values can be calculated from the intercept lines on the Cinh/Θ-axis. This is related to the standard free energy of adsorption (ΔG_{ads}) with the following equation 6:

$$\Delta G_{ads} = -RT\ Ln\ (55.5\ K\ ads) \quad (6)$$

where R is the gas constant and T is the absolute temperature.
Calculated free energies (ΔG_{ads}) are given in Table 4; the negative values of ΔG_{ads} indicate spontaneous adsorption of the two compounds onto the mild steel surface [10] and strong interactions between inhibitors molecules and the metal surface [11]. In the present study, the estimated ΔG_{ads} values are higher than -40 kJ/mol indicate that the adsorption mechanism of the two compounds may be a chemisorption.

Thermodynamically, ΔG_{ads} related to the standard enthalpy and entropy of the adsorption process, ΔH_{ads} and ΔS_{ads}, respectively, via Eq. (7):

$$\Delta G_{ads} = \Delta H_{ads} - T.\Delta S_{ads} \quad (8)$$

and the standard enthalpy of adsorption (ΔH_{ads}) can be calculated according to the Van't Hoff equation [10]:

$$LnK_{ads} = -\frac{\Delta H_{ads}}{RT} + Const \quad (9)$$

A plot of *Ln* K_{ads} versus 1000/T gives a straight line, as shown in Fig. 5. The slope of the straight line is ΔH_{ads} /R and the intercept is ($\Delta S_{ads}/R$ + ln$\frac{1}{C_{H2O}}$). The value of ΔH_{ads} and ΔS_{ads} are given in Table 4.

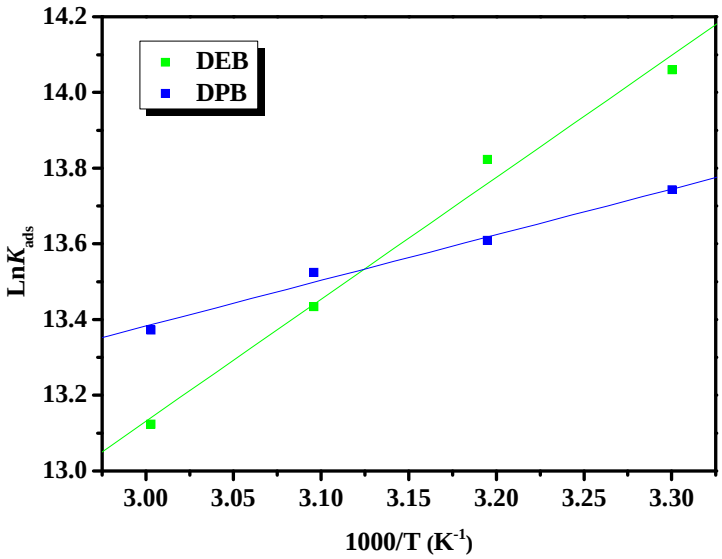

Fig. 5. Plots of Ln K_{ads} Vs 1/T for the inhibition of corrosion of mild steel in 1 M HCl with DPB and DEB

The thermodynamic parameters (ΔH_{ads} and ΔS_{ads}) can also evaluated using the Gibbs-Helmholtz equation, which is defined as follow in the arranged form [28]:

$$\frac{\Delta G_{ads}}{T} = -\frac{\Delta H_{ads}}{T} + Const \quad (10)$$

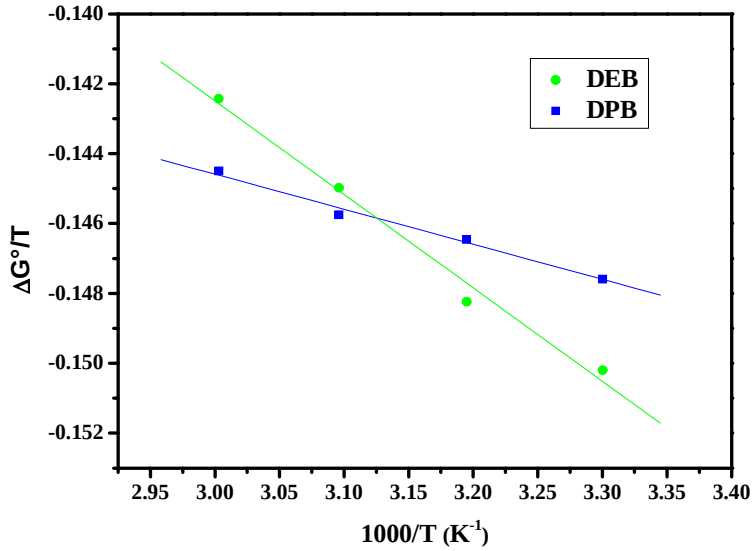

Fig. 6. Plots of ΔG/T Vs 1/T for the inhibition of corrosion of mild steel in 1M HCl with DEB and DPB

Fig. 6 shows the variation of $\Delta G_{ads}/T$ with $1/T$ which gives a straight line with a slope that equals ΔH_{ads}. It can be seen from the figure that $\Delta G_{ads}/T$ decreases with $1/T$ in a linear fashion.
Since the ΔH_{ads} value is negative, the adsorption of inhibitor molecules onto the mild steel surface is an exothermic process, which indicate that the inhibition efficiencies decrease, with increasing the temperature. On the other hand, the adsorption of inhibitor molecules is accompanied by positive values of ΔS_{ads}.

It should be noted that, in an exothermic process, chemisorption is distinguished from physisorption by considering the absolute value of ΔH_{ads}, for the chemisorption process, it approaches 100 kJ/mol, while for the physisorption process, it is less than 40 kJ /mol [29-31]. But, in this case, the chemisorption is governed by the high values of ΔS_{ads}. From the same table, we can see that the values of ΔH_{ads} obtained by both methods are in good agreement.

Table 3 Adsorption parameters of DPB and DEB for mild steel corrosion in 1M HCl at different temperatures

Inhibitors	Temp. (K)	Langmuir adsorption isotherm		Van't Hoff equation		Gibbs Helmholtz equation
		K_{ads}	ΔG_{ads} (kJ mol^{-1})	ΔH_{ads} (kJ mol^{-1})	ΔS_{ads} (J mol^{-1}K^{-1})	ΔH_{ads} (kJ mol^{-1})
DPB	303	1276994	-45.51	-26.77	62.18	-26.75
	313	1007123	-46.40			
	323	682687	-46.83			
	333	500325	-47.43			
DEB	303	929817	-44.72	-10.03	114.5	-10.03
	313	813338	-45.84			
	323	746915	-47.08			
	333	641737	-48.12			

3.2. Electrochemical Measurements

3.2.1. Potentiodynamic Polarization Studies

The potentiodynamic polarization measurements were carried out to study the kinetics of the cathodic and anodic reactions. Fig. 7 shows the results of the effect of DPB inhibitor on the cathodic as well as anodic polarization curves of mild steel in 1M HCl respectively. It is evident from the figure that both reactions were suppressed with the addition of the inhibitor. This suggests that the two reduced the anodic dissolution reactions as well as retarded the hydrogen evolution reactions on the cathodic sites.

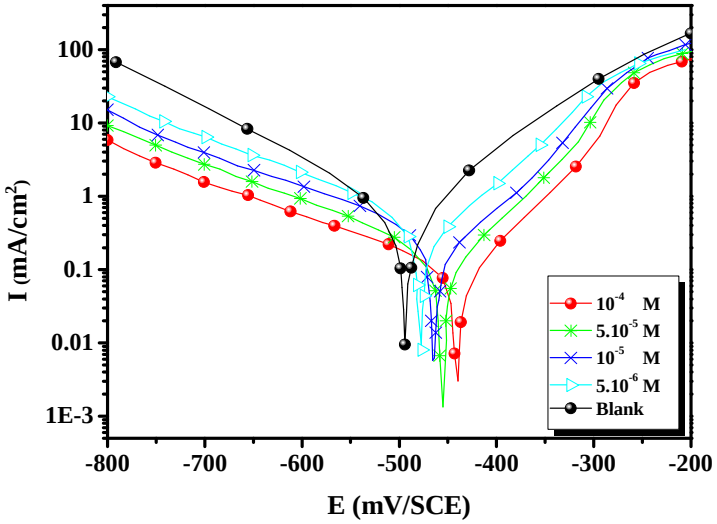

Fig. 7. Polarisation curves of carbon steel in 1 M HCl for various concentrations of selected DPB at 30°C

Electrochemical corrosion kinetic parameters namely corrosion potential (E_{corr}) and corrosion current density (I_{corr}) obtained from the extrapolation of the cathodic polarization curves are listed in Table 4. The corrosion current density (I_{corr}) decreased by the increase in the adsorption of the inhibitor with increasing inhibitor concentration. The inhibition efficiency increases with increase in the inhibitor concentration was calculated by the I_{corr} values and listed in Table 4. According to Ferreira et.al [32], Li et al. [33] and Shukla et al. [34], if the displacement in corrosion potential is more than 85 mV with respect to the corrosion potential of blank solution, the inhibitor can be consider as a cathodic or anodic type. In present study, displacement was 58 mV with respect to the corrosion potential of the uninhibited sample which indicates that the studied inhibitors is a mixed type of inhibitors.

Also, the Tafel plots indicate that the mechanism of hydrogen reduction is activation control. The presence of tested inhibitors does not affect the cathodic Tafel slope, indicating that the mechanism of H^+ reduction is not modified with the DEB and DPB concentration. Also, the corrosion potential is almost constant in the presence of the inhibitors. The inhibitor molecules decrease the surface area of corrosion and only cause inactivation of a part of the surface with respect to the corrosion medium. The inhibition efficiency reaches 92.37% and 88.12 % at 10^{-4} M of DPB and DEB, respectively. This phenomenon is interpreted by the adsorption of the molecules on steel surface leading to the increase of the surface coverage.

Table 4. Corrosion parameters for corrosion of mild steel with concentrations of the inhibitors in 1M HCl by Potentiodynamic polarization method at 303K

Inhibitor	Conc. (M)	$-E_{corr}$ (mV/SCE)	$-\beta_c$ (mV dec^{-1})	I_{corr} ($\mu A\ cm^{-2}$)	η_{Tafel} (%)
Blank	1.0	496	162	564	-
DEB	10^{-4}	438	186	43.0	**92.37**
	5.10^{-5}	457	183	66.3	88.24
	10^{-5}	467	174	77.7	86.22
	5.10^{-6}	480	176	119.1	78.88
DPB	10^{-4}	441	167	67.0	**88.12**
	5.10^{-5}	458	159	80.2	85.78
	10^{-5}	460	181	108.0	80.85
	5.10^{-6}	477	165	133.2	76.38

3.2.2. AC Impedance Spectroscopic Studies

Nyquist representation of the EIS study of mild steel in 1M HCl in absence and presence of different concentrations of DEB were presented in figure 8. The large capacitive loop attributed to the adsorption of the inhibitor molecule [34-35].

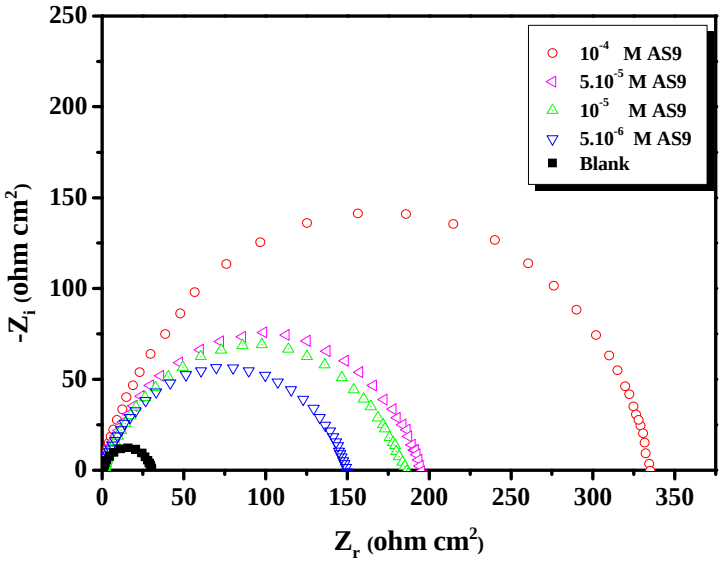

Figure 8. Nyquist curves for mild steel in 1M HCl for selected concentrations of the inhibitor DEB at 303K

The simple equivalent Randle circuit for studies is shown in Fig. 9, where R_s represents the solution and corrosion product film; the parallel combination of resister, R_t and capacitor C_{dl} represents the corroding interface. The existence of single semi-circle showed the single charge transfer process. Depression from the perfect semi-circle is due to the inhomogeneous nature of the metal surface arising from the surface roughness or the interfacial phenomenon [36].

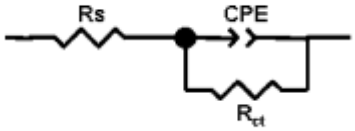

Figure 9. Equivalent electrical circuit corresponding to the corrosion process on the carbon steel in hydrochloric acid

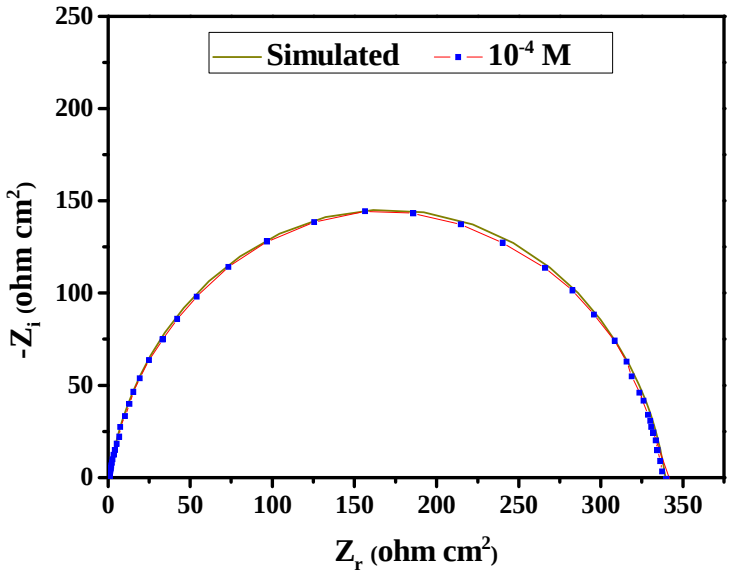

Figure 10. EIS Nyquist plots for carbon steel in 1 M HCl with 10^{-4}M DEB interface: dotted lines experimental data; dashed line calculated

Fig. 10 gives the fitted EIS Nyquist plot for carbon steel in 1 M HCl with 10^{-4}M DPB interface using the above Equivalent electrical circuit.

The increase in R_t value due to the addition of inhibitors in comparison to the absence of inhibitors is attributed to the formation of protective film on the metal/solution interface. These observations suggest that the inhibitors molecules function by adsorption at metal surface thereby causing the decrease in C_{dl} values and increase in R_t values [34-37].

The charge transfer resistance (R_t) and the interfacial double layer capacitance (C_{dl}) derived from these curves are given in table 6. Inhibition efficiency was calculated by the using the charge transfer resistance values. The results obtained from the EIS studies showed good agreement with the results obtained from the Tafel polarization and weight loss measurements.

Table 5. AC-impedance parameters for corrosion of mild steel for selected concentrations of the inhibitors in 1M HCl at 303K

Inhibitor	Conc (M)	R_{ct} (Ω cm^2)	n	$Q\times10^{-4}$ ($s^n\ \Omega^{-1}cm^{-2}$)	C_{dl} (μF cm^{-2})	η_z (%)	Θ
Blank	1.0	29 .35	0.91	1.7610	91.63	-	-
DPB	10^{-4}	338.4	0.90	0.3979	24.65	**91.33**	0.913
	5.10^{-5}	193.0	0.91	0.6370	41.23	84.79	0.847
	10^{-5}	183.0	0.92	0.7308	50.22	83.96	0.839
	5.10^{-6}	148.0	0.90	0.9210	57.15	80.17	0.801
DEB	10^{-4}	262.8	0.90	0.4611	28.24	**88.83**	0.888
	5.10^{-5}	197.5	0.92	0.6064	41.27	85.14	0.851
	10^{-5}	163.1	0.91	0.7250	46.74	82.00	0.820
	5.10^{-6}	106.8	0.93	0.9079	64.05	72.17	0.721

3.3. SEM Analysis of metal Surface

Scanning electron microscopy photographs obtained for mild steel surface after immersion in 1 M HCl solution for 6 h at 303 K in the absence and presence of DEB (10^{-4}M) are shown in Fig. 11. The steel surface was greatly corroded in HCl solution in absence of DEB (Fig. 10b). On the other hand, it can be observed that the addition of DEB results in formation of a protective layer on the surface which greatly reduces the corrosion rate (Fig. 10c).

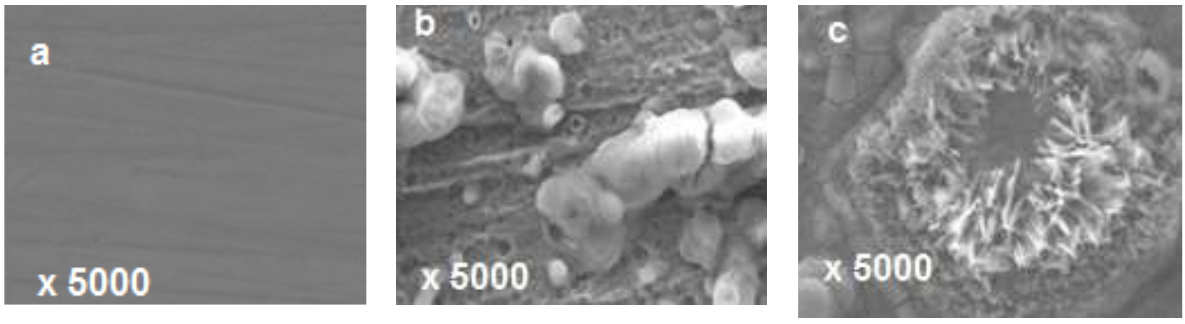

Fig.13. SEM images of mild steel (x5000): (a) unexposed, (b) exposed in 1M HCl and (c) exposed in 1M HCl in the presence of 10^{-4}M of DEB for 6h at 303K

3.4. Quantum chemical calculations

3.4.1. Global reactivity descriptors

The frontier orbital (highest occupied molecular orbital HOMO and lowest unoccupied molecular orbital LUMO) of a chemical species are very important in defining its reactivity. Fukui first recognized this. A good correlation has been found between the speeds of corrosion and E_{HOMO} that is often associated with the electron donating ability of the molecule. Survey of literature shows that the adsorption of the inhibitor on the metal surface can occur on the basis of donor–acceptor interactions between the π-electrons of the heterocyclic compound and the vacant d-orbital of the metal surface atoms [38], high value of E_{HOMO} of the molecules shows its tendency to donate electrons to appropriate acceptor molecules with low energy empty molecular orbitals. Increasing values of E_{HOMO} facilitate adsorption and therefore enhance the inhibition efficiency, by influencing the transport process through the adsorbed layer. Similar relations were found between the rates of corrosion and ΔE ($\Delta E = E_{LUMO} - E_{HOMO}$) [39–41]. The energy of the lowest unoccupied molecular orbital indicates the ability of the molecule to accept electrons. The lower the value of E_{LUMO}, the more probable the molecule would accept electrons. Consequently, concerning the value of the energy gap ΔE, larger values of the energy difference will provide low reactivity to a chemical species. Lower values of the ΔE will render good inhibition efficiency, because the energy required to remove an electron from the lowest occupied orbital will be low [42]. Another method to correlate inhibition efficiency with parameters of molecular structure is to calculate the fraction of electrons transferred from inhibitor to metal surface. According to Koopman's theorem [43], E_{HOMO} and E_{LUMO} of the inhibitor molecule are related to the ionization potential (I) and

the electron affinity (A), respectively. The ionization potential and the electron affinity are defined as I = - E_{HOMO} and A = - E_{LUMO}, respectively. Then absolute electronegativity (χ) and global hardness (η) of the inhibitor molecule are approximated as follows [42]:

$$\chi = \frac{IE + EA}{2} \tag{14}$$

$$\eta = \frac{IE - EA}{2} \tag{15}$$

The global electrophilicity index was introduced by Parr [44] and is given by:

$$\omega = \frac{\mu^2}{2\eta} \tag{16}$$

Thus the fraction of electrons transferred from the inhibitor to metallic surface, ΔN, is given by [45]:

$$\Delta N = \frac{\chi_{Fe} - \chi_{inh}}{2\left(\eta_{Fe} + \eta_{inh}\right)} \tag{17}$$

In order to calculate the fraction of electrons transferred, a theoretical value for the electronegativity of bulk copper was used χ_{Fe}= 7eV/mol [43], and a global hardness of, η_{Fe} = 0 eV/mol by assuming that for a metallic bulk I = A, because they are softer than the neutral metallic atoms [46].

Quantum chemical parameters obtained from the calculations which are responsible for the inhibition efficiency of inhibitors, such as the highest occupied molecular orbital (E_{HOMO}), energy of lowest unoccupied molecular orbital (E_{LUMO}), HOMO–LUMO energy gap (ΔE_{H-L}), dipole moment (μ) and total energy (TE), electronegativity (χ), electron affinity (A), global hardness (η), softness (σ), ionization potential (I), The global electrophilicity (ω), the fraction of electrons transferred from the inhibitor to iron surface (ΔN) and the total energy (TE) , are collected in Table 6.

Table 7: The calculated quantum chemical parameters for the neutral inhibitors

Quantum parameters	DPB	DEB
E_{HOMO}	-2.4234	-1.3001
E_{LUMO}	0.3104	-0.0032
ΔE_{H-L}	2.7339	1.2969
μ	1.6499	0.5200
EI%	88.12	92.30
I	2.4234	1.3001
A	-0.3104	0.0032
χ	1.0565	0.6517
η	1.36696	0.64845
σ	0.731548	1.542145
ΔN	2.173984	4.89498
ω	0.9957	0.20849
TE	-15766.2	-12555.9

In Fig. 12, we have presented the frontier molecule orbital density distributions of the studied compounds: HOMO (right); LUMO (left). Analysis of Fig. 12 shows that the distribution of two energies HOMO and LUMO, we can see that the electron density of the HOMO location in the molecules is mostly distributed near the nitrogen (N) indicating that these are the favorite sites for adsorption, while the density LUMO was distributed almost of the entire molecules.

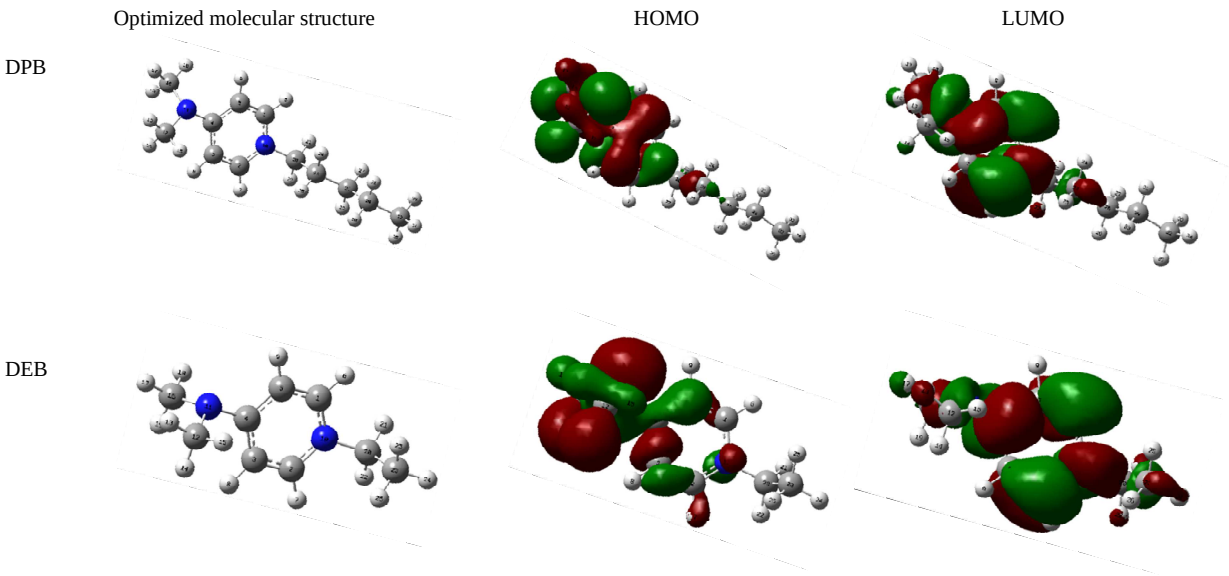

Fig. 12. The optimized structure and calculated HOMO and LUMO molecular orbitals of DPB, DEB, inhibitors using the B3LYP/6-31 G(d,p)

According to the frontier molecular orbital theory (FMO) of chemical reactivity, transition of electron is due to interaction between highest occupied molecular orbital (HOMO) and lowest unoccupied molecular orbital (LUMO) of reacting species [47]. E_{HOMO} is a quantum chemical parameter which is often associated with the electron donating ability of the molecule. High value of E_{HOMO} is likely to a tendency of the molecule to donate electrons to appropriate acceptor molecule of low empty molecular orbital energy [48]. The inhibitor does not only donate electron to the unoccupied d orbital of the metal ion but can also accept electron from the d-orbital of the metal leading to the formation of a feedback bond. The highest value of E_{HOMO} of DPB indicates the better inhibition efficiency.

Therefore, the tendency for the formation of a feedback bond would depend on the value of E_{LUMO}. The lower the E_{LUMO}, the easier is the acceptance of electrons from the d orbital of the metal [41]. Based on the values of E_{LUMO}, the order obtained for the decrease in inhibition efficiency (DPB > DEB) was also similar to the one obtained from experimental results.

The separation energy, $\Delta E = E_{LUMO} - E_{HOMO}$ is an important parameter as a function of reactivity of the inhibitor molecule towards the adsorption on metallic surface. As ΔE decreases, the reactivity of the molecule increases leading to increase the inhibition efficiency of the molecule. The results obtained from quantum chemical calculation are listed in Table 6. The calculations indicate that DPB has the lowest value which means the highest reactivity among the other inhibitor and accordingly the highest inhibition efficiency which agrees well with the experimental observations. The order of reactivity in this case will be: (DPB > DEB).

Absolute hardness and softness are important properties to measure the molecular stability and reactivity. It is apparent that the chemical hardness fundamentally signifies the resistance towards the deformation or polarization of the electron cloud of the atoms, ions or molecules under small perturbation of chemical reaction. A hard molecule has a large energy gap and a soft molecule has a small energy gap [49]. In our present study DPB with low hardness value 0.64845 (eV) compared with other compound have a low energy gap. Normally, the inhibitor with the least value of global hardness (hence the highest value of global softness) is expected to have the highest inhibition efficiency [50]. For the simplest transfer of electron, adsorption could occur at the part of the molecule where softness (σ), which is a local property, has a highest value [39]. DPB with the softness value of 1.542145 has the highest inhibition efficiency.

The most widely used quantity to describe the polarity is the dipole moment of the molecule [51]. Dipole moment is the measure of polarity of a polar covalent bond. It is defined as the product of charge on the atoms and the distance between the two bonded atoms. The total dipole moment, however, reflects only the global polarity of a molecule. For a complete molecule the total molecular dipole moment may be approximated as the vector sum of individual bond dipole moments. The dipole moment (μ in Debye) is another important electronic parameter that results from non-uniform distribution of charges on the various atoms in the molecule. The high value of dipole moment probably increases the adsorption between chemical compound and metal surface [52]. The energy of the

deformability increases with the increase in μ, making the molecule easier to adsorb at the Fe surface. The volume of the inhibitor molecules also increases with the increase of μ. This increases the contact area between the molecule and surface of steel and increasing the corrosion inhibition ability of inhibitors. In our study, there is no direct relationship between the EI (%) and the dipole moment.

In literature it has been reported that the values of ΔN show inhibition effect resulted from electrons donation [43, 53]. According to Lukovits's study [53], if the value of ΔN < 3.6, the inhibition efficiency increased with increasing electron donating ability of inhibitor at the metal surface. Also it was observed [54] that inhibition efficiency increased with increase in the values of ΔN. In our study, the results, as reported in Table 6, show that the order of electron transfer is such that DPB > DEB, which also confirms that DPB has the highest tendency to donate electrons and therefore the highest tendency to bind onto the metal surface.

The total energy calculated by quantum chemical methods is also a beneficial parameter. The total energy of a system is composed of the internal, potential, and kinetic energy. Hohenberg and Kohn [55] proved that the total energy of a system including that of the many body effects of electrons (exchange and correlation) in the presence of static external potential (for example, the atomic nuclei) is a unique functional of the charge density. The minimum value of the total energy functional is the ground state energy of the system. The electronic charge density which yields this minimum is then the exact single particle ground state energy. In our study the total energy of the best inhibitor DPB is equal to -12555.9 eV, this value is lower than that of the compound DEB.

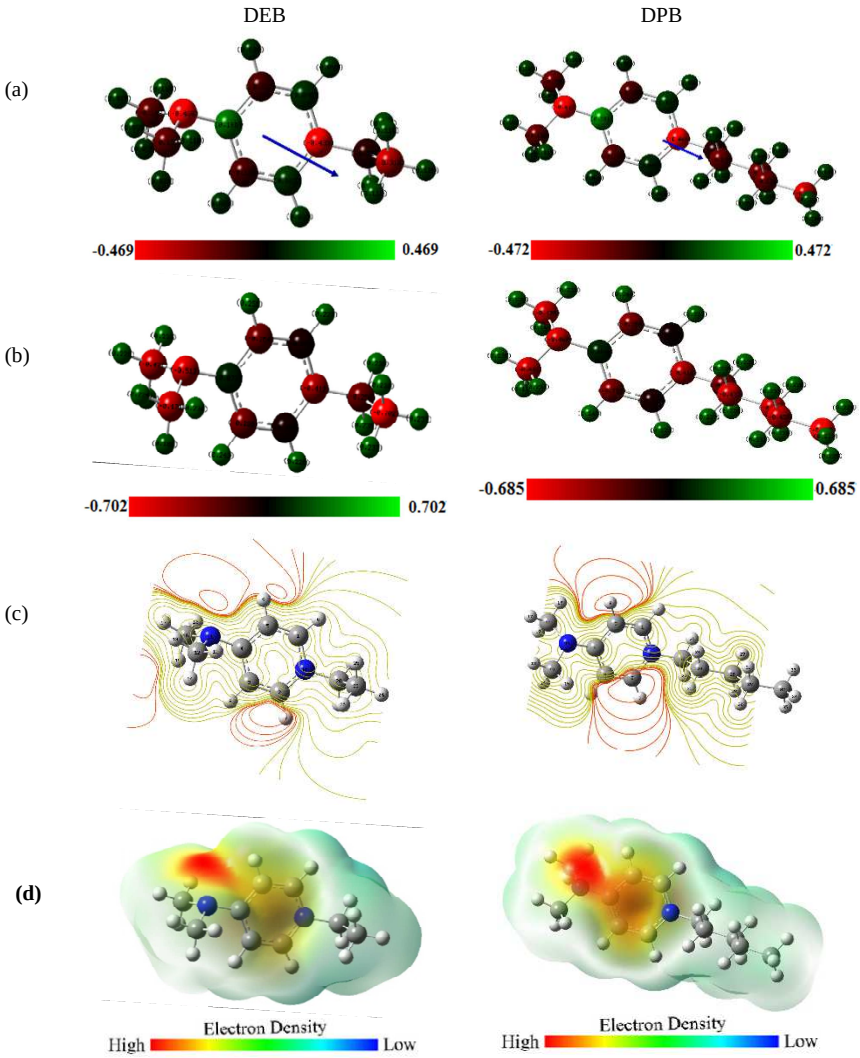

Fig. 13. Electrostatic properties of DPB and DEB: (a) The dipole moment with the Mulliken charge populations, (b) The NBO atomic charges, (c) and (d) The contour and isosurface representation of electrostatic potential respectively

3.4.2. Molecular electrostatic potential and Fukui functions

In order to investigate the reactive sites in the tested inhibitors, Molecular electrostatic potential (MESP) maps provide a visual method to understand the region of the electrophilic attack, nucleophilic attack and the electrostatic potential zero regions[56]. The total electron density surface mapped with molecular electrostatic potential (MESP) and Electrostatic potential contour surface of DEB and DPB are shown in Fig. 13, respectively. The different values of the electrostatic potential were demonstrated with the help of different colors which are red, yellow, green, light blue and blue. The red and yellow colors suitable for the negative parts of the MESP are linked to electrophilic reactivity, blue colors suitable for the positive parts to the nucleophilic reactivity and the green color represents the electrostatic potential zero region[57, 58]. According to the ESP contour surface and MESP of studied inhibitors, the negative regions are electrophilic active regions are mainly observed over the nitrogen atoms. The positive regions are the nucleophilic regions and these are over the some carbon atoms of the title molecules. These observations have also been supported by the evidence Mulliken charges, natural bond orbital analysis and Fukui functions.

Fukui functions are used to measure the local reactivity of the inhibitors molecules and indicate their chemical reactivity for nucleophilic and electrophilic nature[59, 60]. Using a scheme of finite difference approximations, this procedure condenses the values around each atomic site into a single value that characterizes the atom in the molecule. With this approximation, the condensed Fukui function becomes[61]:

$$f_k^+ = P_k(N+1) - P_k(N) \quad (18)$$

$$f_k^- = P_k(N) - P_k(N-1) \quad (19)$$

Where $P_k(N+1)$, $P_k(N)$, $P_k(N-1)$ represent charge values of atom k for anion, neutral, and cation, respectively. The preferred site for nucleophilic attack is the atom in the molecule where the value of f_k^+ is the highest while the preferred site for electrophilic attack is the atom in the molecule where the value of f_k^- is the highest[62]. The values of calculated Fukui functions based on natural population analysis, given in Table 7. In DEB and DPB, atoms C1, C2, C4, and N10, present the highest values of f_k^+, where are the most susceptible sites for nucleophilic attacks. On the other hand, in DEB, atoms C1, C2, C4, and N10, in DPB, atoms C1, C2, C4, N10, and N11, are the susceptible sites for electrophilic attacks as they present the highest values of f_k^-. The information obtained from the Fukui condensed function entirely agrees with the analysis of the FMO and ESP.

Table 7 Values of the Fukui functions according with Eqs. (18)- (19)

Atom	DEB		DPB		Atom	DEB		DPB	
	f_k^-.	f_k^+	f_k^-.	f_k^+		f_k^-.	f_k^+	f_k^-.	f_k^+
1 C	0.137	0.126	0.127	0.117	19 H	0.023	0.023	0.058	0.013
2 C	0.125	0.117	0.116	0.128	20 C	-0.022	-0.019	-0.005	-0.017
3 C	0.013	-0.005	-0.018	0.004	21 H	0.033	0.037	0.025	0.048
4 C	0.211	0.253	0.179	0.204	22 H	0.033	0.036	0.025	0.048
5 C	0.007	-0.007	-0.040	0.026	23 C	-0.003	-0.003	-0.004	0.001
6 H	0.048	0.046	0.041	0.046	24 H	0.040	0.045	0.008	0.009
7 H	0.046	0.046	0.041	0.046	25 H	0.011	0.013	0.008	0.008
8 H	0.045	0.044	0.035	0.040	26 H/C	0.012	0.013	-0.012	0.005
9 H	0.047	0.047	0.027	0.048	27 H			0.012	0.014
10 N	0.097	0.100	0.069	0.091	28 H			0.013	0.014
11 N	0.003	-0.014	0.140	-0.062	29 C			-0.015	0.007
12 C	-0.017	-0.015	-0.022	-0.019	30 H			0.008	0.002
13 H	0.039	0.042	0.039	0.024	31 H			0.008	0.002
14 H	0.021	0.020	0.060	0.009	32 C			-0.014	0.005
15 H	0.011	0.012	0.015	0.056	33 H			0.009	0.003
16 C	-0.014	-0.012	-0.023	-0.016	34 H			0.018	0.012
17 H	0.038	0.045	0.042	0.021	35 H			0.009	0.003
18 H	0.012	0.011	0.015	0.055					

3.4.3. NBO analysis and Mulliken charges

The calculation of atomic charges plays an important role in the application of quantum chemical calculations. The charges on the chelating atom give more information about the adsorbability of the inhibitors on the mild steel surface. The higher the negative partial atomic charge of the adsorbed center, the more easily the atom donates its electron to the partially filled or vacant d orbital of the metal[63, 64]. The Mulliken atomic charges on the atoms of the studied molecules with optimized geometry and the direction of the dipole moment vector calculated at the B3LYP/6-31G(d,p) level are presented in Fig. 13, and collected in Table 8.

Table 8 Calculated NBO and Mulliken atomic charges at DFT/ B3LYP/6-31 G(d,p)

Atom	DEB		DPB		Atom	DEB		DPB	
	NBO	Mulliken	NBO	Mulliken		NBO	Mulliken	NBO	Mulliken
1 C	-0.066	0.078	-0.066	0.089	19 H	0.191	0.075	0.191	0.085
2 C	-0.055	0.083	-0.055	0.059	20 C	-0.256	-0.068	-0.252	-0.068
3 C	-0.286	-0.121	-0.286	-0.131	21 H	0.236	0.109	0.235	0.102
4 C	0.077	0.186	0.076	0.231	22 H	0.236	0.108	0.235	0.103
5 C	-0.264	-0.112	-0.264	-0.125	23 C	-0.702	-0.310	-0.471	-0.169
6 H	0.227	0.092	0.226	0.091	24 H	0.237	0.105	0.236	0.105
7 H	0.226	0.092	0.226	0.088	25 H	0.238	0.118	0.236	0.102
8 H	0.243	0.081	0.242	0.078	26 H/C	0.237	0.117	-0.456	-0.168
9 H	0.251	0.085	0.250	0.081	27 H			0.225	0.089
10 N	-0.412	-0.435	-0.408	-0.445	28 H			0.225	0.089
11 N	-0.513	-0.469	-0.513	-0.472	29 C			-0.446	-0.174
12 C	-0.474	-0.153	-0.473	-0.158	30 H			0.227	0.095
13 H	0.224	0.098	0.224	0.101	31 H			0.227	0.095
14 H	0.188	0.073	0.187	0.081	32 C			-0.675	-0.317
15 H	0.234	0.110	0.233	0.114	33 H			0.224	0.102
16 C	-0.471	-0.149	-0.470	-0.158	34 H			0.231	0.102
17 H	0.221	0.097	0.221	0.100	35 H			0.224	0.102
18 H	0.233	0.109	0.232	0.108					

It is clear from Table 8, that all the nitrogen atoms as well as some carbons atoms for both inhibitors carries negative charge centers which are the probable reactive sites, could offer electrons to the mild steel surface to form a coordinate bond. It is worthy to mention that there are more negative charge centers in DPB than in DEB. On the other hand, DPB donates more negative charge to the d-orbitals of Fe than DEB. The direction of the dipole moment for both inhibitors is toward the nitrogen atoms, and the side containing the negative centers. It can be also understand the direction of the dipole moment by considering the electrostatic potential (Fig. 13c-d), which discerns electron density rich regions centered on the nitrogen atoms and some carbon atoms,

Natural bond orbital (NBO) analysis is an essential tool for studying intra and intermolecular bonding interactions among bonds, it is also used to provide a convenient basis for investigating charge transfer or conjugative interactions in molecular systems[65]. NBO analysis was performed using NBO 3.1 program implemented in the Gaussian 03 program with B3LYP/6-31G(d,p) level[66, 67], and the results are presented in Fig. 13 and reported in Table 8. From the resulted values one can conclude that the two nitrogen atoms of the two inhibitors as well as the some carbon atoms bonded to the nitrogen atom possess the highest negative atomic charges suggesting that the tested compounds can effectively inhibit the corrosion of the mild steel through adsorption on its surface via their reactive sites.

CONCLUSION

All the weight loss measurements showed that the **DEB** and **DPB** have excellent inhibition properties against the mild steel corrosion in hydrochloric acid solution. Thermodynamic calculations show that the adsorption process is spontaneous, exothermic in nature. Potentiodynamic polarization measurements showed that the inhibitors act as mixed type of inhibitor. EIS measurements also indicates that the inhibitor performance increase due to the adsorption of molecule on the metal surface. The inhibitors showed maximum inhibition efficiency at 10^{-4} M concentration of the studied compounds. The inhibition efficiencies determined by the above methods are in good agreement. The inhibitors follow the Langmuir adsorption isotherm in the process of adsorption. Surface morphological study with SEM showed that a film of inhibitor is formed on the electrode surface. Quantum chemistry calculation reveals that the substitution of ethyl by pentyl in 4-(dimethylamino)pyridinium bromide gives a decrease in ΔE_{H-L} energy. The great increase of inhibition efficiency due to increase of ΔE_{H-L}, implying the ability of organic molecule to offer free electrons to the metal surface.

Acknowledgment
The authors would like to thank MENA NWC for their financial support for grant no: WIF 04. Also, we would like to extend our thanks to Palestine Water Authority (PWA) and MEDRIC for their support. The support given through an “INCRECYT” research contract to M. Zougagh is also acknowledged.

REFERENCES

[1] V. S. Sastri, Green Corrosion Inhibitors. Theory and Practice, John Wiley & Sons: Hoboken, NJ; **1998**.

[2] H. B. Ouici, M. Belkhouda, O. Benali, R. Salghi, L. Bammou, A. Zarrouk, B. Hammouti, *Res. Chem. Intermed.*, **2015**, 41, 4617.
[3] L .Afia, R. Salghi, A. Zarrouk, H. Zarrok, O. Benali, B. Hammouti, S.S. Al-Deyab, A. Chakir, L.Bazzi, *Port. Electrochim. Acta*. **2012**, 30 (4), 267.
[4] A. Anejjar, A. Zarrouk, R. Salghi, H. Zarrok, D. Ben Hmamou, B. Hammouti, B. Elmahi, S.S. Al-Deyab, *J.Mater. Environ, Sci.* ***2013***,4 (5), 583.
[5] A. Zarrouk, H. Zarrok, R. Salghi, B. Hammouti,F. Bentiss, R. Touir, M. Bouachrine, *J. Mater. Environ.Sci*, **2013**, 4,177.
[6] L. Messaadia, O. ID El mouden , A. Anejjar , M. Messali, R. Salghi, O. Benali, O. Cherkaoui , A. Lallam. *J.Mater. Environ. Sci*, **2015**, 6 (2) ,598-606.
[7] H. Elmsellem, H. Bendaha, A. Aouniti, A. Chetouani, M. Mimouni, A. Bouyanzer. *Mor. J. Chem*. **2014**, 2 (1), 1-9.
[8] M.K. Awad, R.M. Issa, F.M. Atlam, *Mater. Corros,* **2009**, 60, 813.
[9] H. Elmsellem, H. Nacer, F. Halaimia, A. Aouniti, I. Lakehal, A .Chetouani, S. S. Al-Deyab, I. Warad, R.Touzani, B. Hammouti. *Int. J. Electrochem. Sci*., **2014**, 9, 5328 –5351.
[10] O. Benali, L. Larabi, M. Traisnel, L. Gengembra, Y. Harek, *Appl. Surf. Sci*. **2007,** 253**,** 6130.
[11] Benali O., Larabi L., Mekelleche S.M., Harek Y., *J. Mater. Sci.* **2006**, 41, 7064.
[12] D. Ben Hmamou, R. Salghi, A. Zarrouk, O. Benali, F. Fadel, H. Zarrok, B. Hammouti, *Int. J. Ind. Chem*, **2012**, 3, 25.
[13] A. Doner, R. Solmaz, M. Ozcan, G. Kardas, Corros. Sci. **2011**, 53, 2902–2913.
[14] I.B. Obot, Z.M. Gasem, Corros. Sci. **2014**, 83, 359–366.
[15] X. Li, S. Deng, H. Fu, X. Xie, Corros. Sci. **2014**, 78, 29–42.
[16] M.J. Frisch, G.W. Trucks, H.B. Schlegel, G.E. Scuseria, M.A. Robb, J.R. Cheeseman, J.A. Montgomery Jr., T. Vreven, K.N. Kudin, J.C. Burant, J.M. Millam, S.S. Iyengar, J. Tomasi, V. Barone, B. Mennucci, M. Cossi, G. Scalmani, N. Rega, G.A. Petersson, H. Nakatsuji, M. Hada, M. Ehara, K. Toyota, R. Fukuda, J. Hasegawa, M. Ishida, T. Nakajima, Y. Honda, O. Kitao, H. Nakai, M. Klene, X. Li, J.E. Knox, H.P. Hratchian, J.B. Cross, C. Adamo, J. Jaramillo, R. Gomperts, R.E. Stratmann, O. Yazyev, A.J. Austin, R. Cammi, C. Pomelli, J.W. Ochterski, P.Y. Ayala, K. Morokuma, G.A. Voth, P. Salvador, J.J. Dannenberg, V.G. Zakrzewski, S. Dapprich, A.D. Daniels, M.C. Strain, O. Farkas, D.K. Malick, A.D. Rabuck, K. Raghavachari, J.B. Foresman, J.V. Ortiz, Q. Cui, A.G. Baboul, S. Clifford, J. Cioslowski, B.B. Stefanov, G. Liu, A. Liashenko, P. Piskorz, I. Komaromi, R.L. Martin, D.J. Fox, T. Keith, M.A. Al-Laham, C.Y. Peng, A. Nanayakkara, M. Challacombe, P.M.W. Gill, B. Johnson, W. Chen, M.W. Wong, C. Gonzalez, J.A. Pople, Gaussian 03, Revision B. 03, Gaussian Inc, Pittsburgh, PA, **2003**.
[17] Gauss View, Version 3.0, Gaussian Inc., Pittsburgh, PA, **2003**.
[18] A.R.S. Priya, V.S. Muralidharam, A. Subramania, *Corrosion*, **2008**, 64, 541.
[19] I.B. Obot, N.O. Obi-Egbedi, *Mater. Chem.* Phys., **2010**, 122, 325.
[20] I.B. Obot, N.O. Obi-Egbedi, *Corros. Sci.*, **2009**, 51, 276.
[21] M.M. Solomon, S.A. Umoren, I.I. Udosoro, A.P. Udoh, *Corros. Sci.*, **2010**, 52, 1317.
[22] S.A. Umoren, M.M. Solomon, I.I. Udousoro, A.P. Udoh, *Cellulose*, **2010**, 17, 635.
[23] N. M. Guan, I. Xueming, I. Fei, *Mater. Chem. Phys*., **2004**, 86, 59.
[24] A. Zarrouk, B. Hammouti, H. Zarrok, S. S. Al-Deyab, I. Warad, *Res. Chem. Intermed*., **2012**, 38, 1655.
[25] A. Zarrouk, B. Hammouti, H. Zarrok, S.S. Al-Deyab, M. Messali, *Int. J. Electrochem. Sci.*, **2011**, 6, 6261.
[26] I. El Ouali, B. Hammouti, A. Aouniti, Y. Ramli, M. Azougagh, E. M. Essassi, M. Bouachrine, *J. Mater. Envir. Sci*., **2010**, 1, 1.
[27] E.F.Olasehinde, A. S. Adesina, 1, E. O.Fehintola, B. M. Badmus, A. D.Aderibigbe, *J. Appl. Chem. 2 (6)(2012)15-23.*
[28] S. Bilgic, *Mater. Chem. Phys*., **2002**, 76, 52.
[29] K. Tebbji, A. Aouiniti, B. Hammouti, H. Oudda, M. Benkaddour, S. Radi, A. Hahle, Ind. J. Chem.Tech., **2011**, 18, 244-253.
[30] A.M. Badiea, K.N. Mohana, *Corros. Sci.*, **2009**, 51, 2231.
[31] L. B. Tang, G. N. Mu, G. H. Liu, *Corros. Sci*., **2003**, 45, 2251.
[32] E.S. Ferreira, C. Giancomelli, F.C. Giacomelli, A. Spinelli, *Mater. Chem. Phys.* **2004**, 83, 129.
[33] W.H. Li, Q. He, C.L. Pei, B.R. Hou, *J. Appl. Electrochem*. **2008**, 38, 289.
[34] *S. K Shukla, A. K Singh, M. A. Quraishi, Int. J. Electrochem. Sci.*, **2011,** 6, 5779 – 5791.
[35] S.K. Shukla, M.A. Quraishi, *Corros. Sci.* **2010**, 52, 314.
[36] S.K. Shukla, M.A. Quraishi, *Corros. Sci* **2009**, 51, 1990.
[37] F. Bentiss, M. Traisnel, M. Lagrenee, *Corros. Sci.* **2000**, 42, 127.
[38] A. Domenicano, I. Hargittai, Oxford University Press, New York, **1992**.
[39] W. Li, X . Zhao, F. Liu, J. Deng, B. Hou, *Mater. Corros*. **2009**, 60, 287.
[40] R. Hasanov, M. Sadikoglu, S. Bilgic, *Appl. Surf. Sci.*, **2007**, 253, 3913.
[41] M.A. Amin, K.F. Khaled, S.A. Fadl-Allah, Corros. Sci., **2010**, 52, 140.

[42] H. Wang, X. Wang, H. Wang, L. Wang, A. liu, *J. Mol. Model*., **2007**, 13, 147.
[43] R.G. Pearson, *Inorg. Chem*. **1988**, 27, 734.
[44] V.S. Sastri, J.R. Perumareddi, *Corrosion*. **1997**, 53, 671.
[45] R. G. Parr, L.Szentpaly, S. Liu, *J. Am. Chem. Soc*., **1999**, 121, 1922.
[46] S. Martinez, *Mater. Chem. Phys*., **2002**, 77, 97
[47] M. J. S. Dewar, W. Thiel, *J. Am. Chem. Soc*., **1977**, 99, 4899.
[48] A.Y. Musa, A. H. Kadhum, A. B. Mohamad, A.b. Rohoma, H. Mesmari, *J. Mol. Struct*., **2010**, 969, 233.
[49] G. Gece, S. Bilgic, *Corros. Sci*., **2009**, 51, 1876.
[50] N.O. Obi-Egbedi, I.B. Obot, M.I. El-Khaiary, S.A. Umoren, E.E. Ebenso, *Int. J. Electrochem. Sci*., **2011**, 6, 5649.
[51] E.E. Ebenso, D.A. Isabirye, N.O. Eddy, *Int. J. Mol. Sci*., **2010**, 11, 2473.
[52] O. Kikuchi, *Quant. Struct.-Act. Relat*., **1987**, 6, 179.
[53] X. Li, S. Deng, H. Fu, T. Li, *Electrochim. A*cta., **2009**, 54, 4089.
[54] I. Lukovits, E. Kalman, F. Zucchi, *Corrosion*., **2001**, 57, 3.
[55] H. Ju, Z.P. Kai, Y. Li, *Corros. Sci*., **2008**, 50, 865.
[56] A. Lesar et I. Milošev, *Chem. Phys. Lett*., **2009**, 483, 4‑6, 198‑203.
[57] N. A. Wazzan, J. Ind. Eng. Chem., **2015**, 26, 291‑308.
[58] R. T. Ulahannan, C. Y. Panicker, H. T. Varghese, R. Musiol, J. Jampilek, C. Van Alsenoy, J. A. War, et S. K. Srivastava, *Spectrochim. Acta. A. Mol. Biomol. Spectrosc*., **2015**, 151, 184‑197.
[59] J. Saranya, P. Sounthari, K. Parameswari, et S. Chitra, *Measurement*, **2016**, 77, 175‑186.
[60] S. K. Saha, P. Ghosh, A. Hens, N. C. Murmu, et P. Banerjee, Phys. E Low-Dimens. *Syst. Nanostructures*, **2015**, 66, 332‑341.
[61] Y. Sasikumar, A. S. Adekunle, L. O. Olasunkanmi, I. Bahadur, R. Baskar, M. M. Kabanda, I. B. Obot, et E. E. Ebenso, *J. Mol. Liq*., **2015**, 211, 105‑118.
[62] N. Karakus et K. Sayin, J. *Taiwan Inst. Chem. Eng.*, **2015**, 48, 95‑102.
[63] M. Yadav, S. Kumar, N. Tiwari, I. Bahadur, et E. E. Ebenso, *J. Mol. Liq*., **2015**, 212, 151‑167.
[64] J. Bhawsar, P. K. Jain, et P. Jain, *Alex. Eng. J*., **2015**, 54 (3), 769‑775.
[65] K. Ramya, R. Mohan, K. K. Anupama, et A. Joseph, *Mater. Chem. Phys.*, **2015**, 149‑150, 632‑647.
[66] R. J. Xavier et E. Gobinath, *Spectrochim. Acta. A. Mol. Biomol. Spectrosc*., **2012**, 86, 242‑251.
[67] B. D. Mert, A. O. Yüce, G. Kardaş, et B. Yazıcı, *Corros. Sci.*, **2014**, 85, 287‑295.